Microfluid Nanofluid (2007) 3:283–298
DOI 10.1007/s10404-006-0122-7

RESEARCH PAPER

Simulation and parametric study of a novel multi-spray emitter for ESI–MS applications

A. K. Sen · J. Darabi · D. R. Knapp

Received: 9 May 2006 / Accepted: 20 August 2006 / Published online: 19 October 2006

Abstract In this work, we propose a novel carbon nanofiber (CNF) emitter for electrospray ionization (ESI)–mass spectrometry (MS) applications. The proposed emitter comprises an array of CNFs around the orifice of a microscale capillary. The electrospray ionization process is simulated using a CFD code based on Taylor–Melcher leaky-dielectric formulations for solving the electrohydrodynamics and volume-of-fluid (VOF) method for tracking the interface. The code is validated for a conventional multiple electrospray emitter and then applied to simulate the CNF emitter model. The modeling results show that under steady state condition, individual cone-jets are established around each of the CNFs resulting in an array of electrosprays. The approach being taken to fabricate the CNF emitter is briefly discussed. Effects of geometrical parameters including aspect ratio of CNFs, total number of CNFs and distribution pattern of the CNFs on the electrospray performance are studied. The influence of operating parameters such as flow rate, potential difference and physical properties of the solvent on the electrospray behavior is thoroughly investigated. The spray current, 'onset' potential and jet diameter are correlated with total number and distribution of CNFs and physical properties of the liquid. The correlation results are compared with the available results in the literature. Higher spray current and lower jet diameter indicate that the device can perform equivalent to nanospray emitters while using a micro-scale orifice. This allows higher sample throughput and eliminates potential clogging problem inherent in nano-capillaries.

Keywords Carbon nanofiber · Electrospray ionization–mass spectrometry · Taylor–Melcher leaky-dielectric formulations · Electrohydrodynamics · Volume of fluid

A. K. Sen · J. Darabi (✉)
MEMS and Microsystems Laboratory,
Department of Mechanical Engineering,
University of South Carolina, 300 Main Street,
Columbia, SC 29208, USA
e-mail: darabi@engr.sc.edu
URL: http://www.me.sc.edu/darabi

D. R. Knapp
Department of Pharmacology,
Medical University of South Carolina,
173 Ashley Avenue, Charleston, SC 29425, USA

1 Introduction

The formation of electrospray from a capillary by applying a high electric potential across its orifice is a well known technique originally demonstrated by Zeleny (1914, 1917). The indication of Dole et al. (1968), Clegg and Dole (1971) and Fenn et al. (1989) that electrospray can be used for atomization of large bio-compounds spurred further investigations into this technique. Single-jet atomization that requires less energy is a more common method of electrospray and has been widely studied. In the last few years, modeling and experimental works on several novel single-jet electrospray emitters have been reported (Arscott et al. 2004; Amirkhani et al. 2004; Wang et al. 2004; Trapp et al. 2005; Griss et al. 2002; Kim and Knapp 2001; Jian et al. 2004). The authors have previously published modeling and experimental investigations on a carbon fiber based single-jet emitter which has

several advantages over conventional single-jet emitters (Sen et al. 2006). However, low liquid throughput and less ion current of such emitters have limited their applicability. Use of a combination of several single-jet emitters is operationally and technically complex. Multiple electrospray emitters have several advantages over single-spray emitters in terms of high sample throughput and improved mass spectrometry sensitivity and hence, they are becoming more attractive options for generating electrosprays.

Development of several multiple electrospray emitters have been reported in the last few years. A schematic diagram of a typical multiple cone-jet electrospray process is depicted in Fig. 1. Huberman et al. (1968) reported a less compact multi-injector with holes instead of needles. Rulison and Flagan (1993) used a linear array of capillary tubes placed parallel to each other to achieve an increased liquid throughput rate. Amekinders and Jones (1999) published an electrospray atomizer with several emitters in the form of serrated channels equidistantly arranged on a tip. Recently, Schultz and Corso (2000) proposed a microfabricated emitter array which can be fabricated on a silicon wafer using photolithographic patterning and plasma etching technique. This technique made system integration for high-throughput applications possible where each emitter can be connected to an individual sample reservoir and operated sequentially. However, the spray nozzles fabricated using such technology can be reliably used only for little more than an hour. More recently, Tang et al. (2001) reported a micro-electrospray emitter array fabricated from a polycarbonate substrate using a laser ablation method that offers extended lifetime and higher sensitivity. Regele et al. (2002) investigated an array of four capillary nozzles with an intention to increase liquid throughput without increasing the size of the droplets produced. In the same work they studied the effects of capillary spacing on the potential required for electrospraying. In addition, a simple electrostatic model is also presented to support the experimental results. Bocanegra et al. (2003) presented a multiple electrospray atomizer that uses holes drilled on a hydrophobic plate instead of conventional tips. In this case the curvature of the meniscus sticking out from the hole provides an intensified electric field required for electrospraying. Deng et al. (2006) proposed a compact microneedle injector microfabricated in a hexagonal pattern on a silicon thin plate. Duby et al. (2006) reported an inexpensive multiplexed electrospray system that results in multiple stable cone-jets emanating from a single capillary under certain conditions. Recently, Kaiser et al. (2003) investigated multiple electrosprays coupled with catalytic meshes acting as ground electrodes for a combustor design. The behavior of electrospray is examined at elevated temperature environments and the electrosprays in the combustor were visualized using planar laser-induced fluorescence. Using the novel electrospray-assisted combustor it was possible to achieve clean and highly efficient combustion.

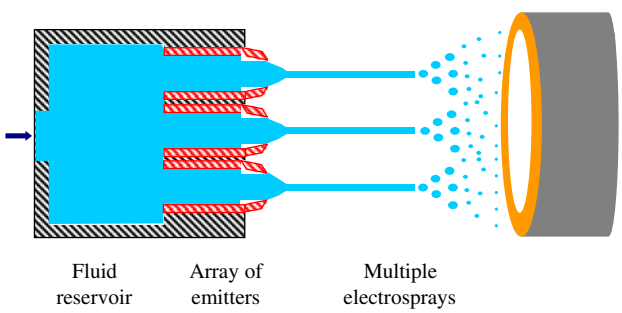

Fig. 1 A typical multiple cone-jet electrospray process

Most of the works on multiple electrospray emitters are based on experiments or theoretical analysis. Recently, Yoon et al. (2001) simulated the multi-jet mode of electrospray using the boundary element method (BEM) to investigate oscillations and instabilities in electrosprays. This is believed to be the first modeling work in studying multiple cone-jet electrospray; however, the governing equations were oversimplified.

Carbon nanofibers, when subjected to an electric field, can generate a high electric field at their sharp tip. The CNFs grown around the orifice of a microscale capillary can serve as emitter points for generating electrosprays. Numerous techniques have been proposed for growing CNFs, including arc-discharge, laser ablation and chemical vapor deposition (Ebbesen and Ajayan 1992; Thess et al. 1996). However, only few techniques can be utilized for controlled growth directly on a substrate (Ren et al. 1998; Merkulov et al. 2000; Chhowalla et al. 2001). Controlled growth of CNFs on silicon and thermoplastic substrates using plasma enhanced chemical vapor deposition (PECVD) has been demonstrated (Hofmann et al. 2003; Ryu et al. 2003). Recently, growth of vertically aligned carbon nanofibers at lower temperature (~120°C) on plastic substrates has been reported (Hofmann et al. 2003; Melechko et al. 2003).

In this work, we propose the concept of a novel multiple cone-jet electrospray emitter based on an array of carbon nanofibers vertically grown around the orifice of a microscale thermoplastic capillary. CFD simulations were performed to study the feasibility of the idea and investigate the performance of the CNF

emitter with respect to several geometric and operational parameters. A computational fluid dynamics code (Flow-3D) was utilized to simulate the electrospray process. The approach being considered for microfabrication of the CNF emitter is briefly discussed. The influence of emitter geometry, flow rate, applied voltage and liquid properties on the electrospray performance of the emitter is thoroughly investigated. The spray current, 'onset' potential and jet diameter are correlated with total number and distribution of CNFs and physical properties of the liquid. The correlation results are compared with the available results in the literature. In the following section, theory of electrohydrodynamic flows is briefly discussed. Then, validation of the CFD code for a conventional multiple electrospray emitter is reported. Furthermore, 3-D simulation results for the CNF-based model is presented and discussed. Then, results of the parametric study of the electrospray performance of the CNF emitter is presented and discussed. Finally, the fabrication approach is briefly discussed.

2 Theory

In this section, theory of the electrospray process is briefly discussed. A detailed description is previously reported in (Sen et al. 2006). The formulations for the cone-jet phase of the electrospray process include Navier–Stoke's equations for the fluid flow and Maxwell's equation controlling the electromagnetic phenomena. The aqueous solutions of bio-samples used in electrospray processes are characterized by low electrical conductivity. For such leaky-dielectric fluids, magnetic forces are negligible and Maxwell's equations are reduced to the electroquasistatic limit falling in the realm of electrohydrodynamics (Castellanos 1998).

In the code, the EHD formulations are based on the Taylor–Melcher leaky dielectric fluid model (Saville 1997) and two different fluids are analyzed: liquid sample and electrospray medium. The present model assumes negligible bulk free charge density and the electric field is assumed to be irrotational and divergence-free throughout the computational domain. At the interface, the flow and electric fields are coupled and to balance the force developed due to the tangential component of the electric field acting on the interface, viscous flow is developed. The various forces acting on a multiple cone-jet interface are shown pictorially in Fig. 2.

The governing equation for the electric field throughout the computational domain is

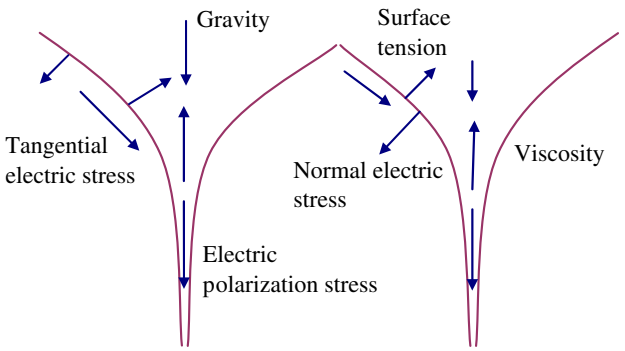

Fig. 2 Distribution of forces on a multiple cone-jet

$$\nabla^2\phi = 0. \tag{1}$$

At the interface, the tangential component of the electric field $\vec{E} = -\nabla\phi$ is continuous and there is a jump of the electric field in the normal direction, which is proportional to the interfacial charge density q,

$$\vec{n}\cdot(\varepsilon_{\mathrm{l}}\nabla\phi_{\mathrm{l}} - \varepsilon_{\mathrm{m}}\nabla\phi_{\mathrm{m}}) = q \tag{2}$$

$$\vec{t}_i\cdot(\varepsilon_{\mathrm{l}}\nabla\phi_{\mathrm{l}} - \varepsilon_{\mathrm{m}}\nabla\phi_{\mathrm{m}}) = 0, \tag{3}$$

where ϕ is the electric potential, $\vec{n}$ is the unit normal of the interface directed in to the electrospray medium, $\vec{t}_i$ represents either of two orthogonal tangent vectors embedded in the surface. ε_{l} and ε_{m} are dielectric constant of liquid and the medium, respectively. The accumulation of interfacial charge density $q$is represented by the charge conservation equation,

$$\frac{\mathrm{d}q}{\mathrm{d}t} = -\vec{n}\cdot\sigma(\nabla\phi_{\mathrm{l}}), \tag{4}$$

where $\mathrm{d}/\mathrm{d}t$ is the Lagrangian derivative and σ is the electrical conductivity of the liquid. The free charges accumulated at the interface induce an electric field normal to its surface which results in normal (T_{n}) and tangential (T_{t}) stresses acting on the interface,

$$T_{\mathrm{n}} = \frac{1}{2}\left[\varepsilon_{\mathrm{l}}(\vec{n}\cdot\nabla\phi_{\mathrm{l}})^2 - \varepsilon_{\mathrm{m}}(\vec{n}\cdot\nabla\phi_{\mathrm{m}})^2\right] \tag{5}$$

$$T_{\mathrm{t}} = -q(\vec{t}_i\cdot\nabla\phi). \tag{6}$$

Assuming the liquid to be incompressible (of constant density ρ) and of constant viscosity η, its motion is described by the continuity and momentum conservation equations,

$$\nabla\cdot\vec{u} = 0 \tag{7}$$

$$\rho\frac{\mathrm{d}\vec{u}}{\mathrm{d}t} = -\nabla p + \eta\nabla^2\vec{u} + \vec{f}_{\mathrm{e}} + \rho\vec{g}, \tag{8}$$

where $\vec{u}$ is the flow velocity, p is the fluid pressure and $\vec{f}_e$ is the electromechanical force. The expression for the electromechanical force can be derived from thermodynamic considerations (Melcher 1981),

$$\vec{f}_e = \nabla \cdot \vec{T}^e = \rho_e \vec{E} - \frac{1}{2}\left|\vec{E}\right|^2 \nabla\varepsilon + \nabla p_{st}, \tag{9}$$

where $\vec{T}^e$ is the electrical stress tensor, ρ_e is the net free charge density, and $p_{st} = \frac{1}{2}(\varepsilon - \varepsilon_0)\left|\vec{E}\right|^2$, is known as the electrostrictive pressure, where ε and ε_0 are the permittivity of the liquid and vacuum, respectively. The first term in Eq. 9, known as the Coulomb force, is the strongest EHD force and is the force per unit volume on a medium containing free electric charge. The second term, called the dielectrophoretic force, arises due to the force exerted by an electric field on a non-homogeneous dielectric fluid. The third term represents the electromechanical force density due to the non-uniformity of the electric field. The tracking of the interface is achieved using the volume of fluid (VOF) technique (Hirt and Nichols 1981). In this technique, the time evolution of the interface between the liquid and air is defined by a volume fraction function F such that,

$$\frac{dF}{dt} + \vec{u} \cdot \nabla F = 0 \tag{10}$$

The above equation represents the kinematic condition at the interface. The interface is tracked using the following conditions:

$$F(x,y,z,t) = \begin{cases} 0 & \text{outside the liquid} \\ 1 & \text{inside the liquid} \\ >0, <1 & \text{on the free surface.} \end{cases} \tag{11}$$

The electrospray current (I) is calculated using the following relation (Hartman et al. 1999),

$$\begin{aligned} I &= I_{\text{conduction}} + I_{\text{convection}} \\ &= \pi R_s^2 \vec{E}_z \sigma + 2\pi R_s \vec{u}_z q, \end{aligned} \tag{12}$$

where R_s is the jet radius, $\vec{E}_z$ is the electric field on the surface of the jet along z-direction, $\vec{u}_z$ is the velocity of jet in z-direction and q is the surface charge density.

3 Validation model

The code is validated for a conventional multiple cone-jet electrospray emitter reported by Tang et al. (2001). The geometry of the emitter is shown in Fig. 3. It comprises an array of nine emitters on a 1 mm thick polycarbonate sheet. Figure 4 shows schematic of the validation model. The separation between the emitter and the counter electrode is maintained at 5 mm. A potential difference of 7 kV is applied between the emitter and the counter electrode. The liquid sample is a mixture of MeOH/H_2O/HOAc with the following physical properties: density ρ = 1,030 kg m^{-3}, coefficient of viscosity μ = 0.008 Pa s, coefficient of surface tension γ = 0.037 Nm^{-1}, dielectric constant k = 55 and electrical conductivity σ = 135 μS m^{-1}.

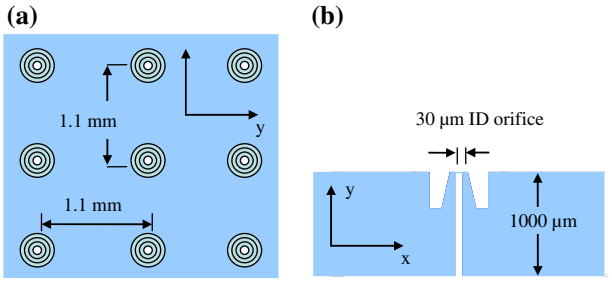

Fig. 3 **a** The multiple electrospray emitter (Tang et al. 2001). **b** Geometry of each electrospray emitter

3.1 Boundary conditions

The boundary conditions for the above model are described with reference to Fig. 5. Boundary 1 (or, Inflow boundary): uniform velocity $\vec{u}_z = u_0$, stagnation pressure boundary condition, which represent presence of an infinite-fluid reservoir continuously supplying fluid

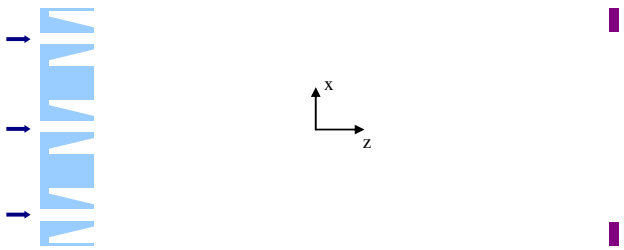

Fig. 4 Cross-sectional view of the validation model

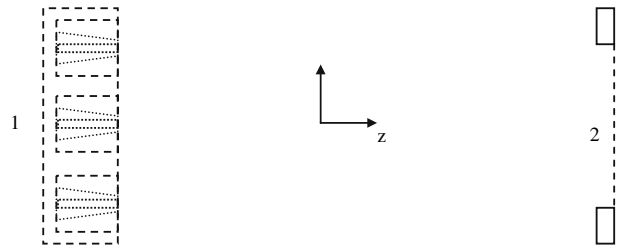

Fig. 5 Boundaries of the computational domain for the validation model

to the nozzle, fluid fraction function $F = 1$, where, $u_0 = Q/A$, A is the total flow cross-sectional area of the nozzles and Q is the total flow rate and $\vec{u}_z$ is the velocity along the z-direction. Boundary 2: continuative boundary conditions, $\frac{\partial \phi}{\partial z} = 0, \frac{\partial \vec{u}_z}{\partial z} = 0, F = 0$. For all other boundaries: symmetric boundary conditions. The counter electrode is assigned a potential $\phi = 0$ and the nozzles are assigned a potential $\phi = \phi_0$, and a dielectric constant $\varepsilon = 2.9$, where ϕ_0 is the potential difference between the emitter and the counter electrode. The boundary conditions at the interface balance surface tension, pressure, viscous stresses and electric stresses (Eqs. 5, 6). The electrical boundary conditions at the interface consider that the tangential components of the electric field $\vec{E}$ are continuous (Eq. 3) and the normal components jump by an amount proportional to the free charge density q (Eq. 2). The kinematic condition at the interface is presented in Eq. 11. The mechanical boundary condition at the interface is governed as follows:

$$\vec{n} \cdot [\vec{T}^{\mathrm{m}} + \vec{T}^{\mathrm{e}}] \cdot \vec{n} = \gamma \nabla \cdot \vec{n}, \tag{13}$$

where $\vec{T}^{\mathrm{m}}$ is the mechanical stress tensor, γ is the coefficient of surface tension. The initial conditions for the liquid in this case are: $\vec{u}_z = u_0, q = 0$ and the fluid fraction function on the interface $F = 0.5$.

3.2 Results and discussion

Figure 6 shows section of a 3-D computational mesh built around the model with (90, 90, 110) cells in (x, y, z) directions. The steady state cone-jet profile and the electric potential contours are shown in Fig. 7. The variation of electrospray current per electrospray as a function of liquid flow rate per electrospray is presented in Fig. 8. It is observed that the electrospray current predicted by the model is consistently higher than that measured in the experiments and the agreement is within 15%. The reason for the mismatch could be due to space charge which is neglected in our simulation. Since the present model is not intended to simulate the jet break-up or droplet fission phases of the ESI process, the jets extend from the apex of the cones to the counter electrode in order to satisfy conservation of mass. A numerical simulation of all regimes of the ESI process including cone-jet, jet break-up and droplet fission is an extremely challenging task. Our future work will be focused on developing a numerical tool to investigate the entire ESI process.

Assuming that each of the electrosprays carries approximately the same current (I/n) and flow rate Q is distributed equally to each of the orifices, the current-flow characteristics for the validation model can be fitted using the following relation,

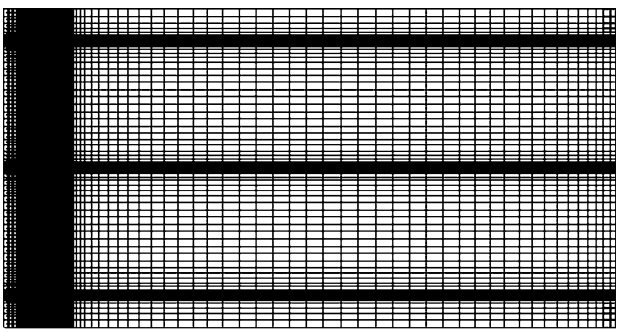

Fig. 6 Non-uniform 3-D mesh with (90, 90, 110) cells in (x, y, z) directions

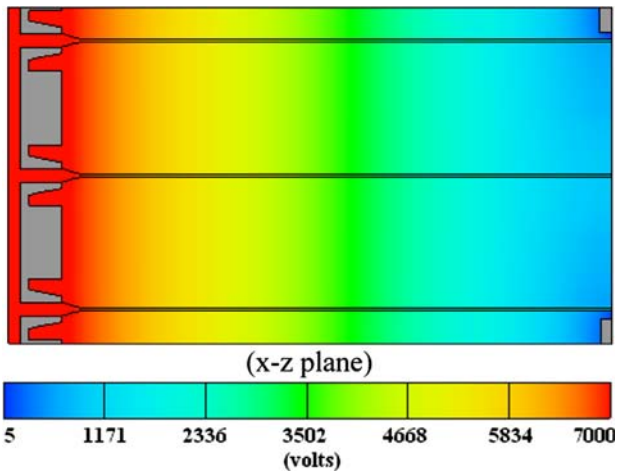

Fig. 7 Cone-jet profile and electric potential contours at a flow rate of 2,000 nl/min

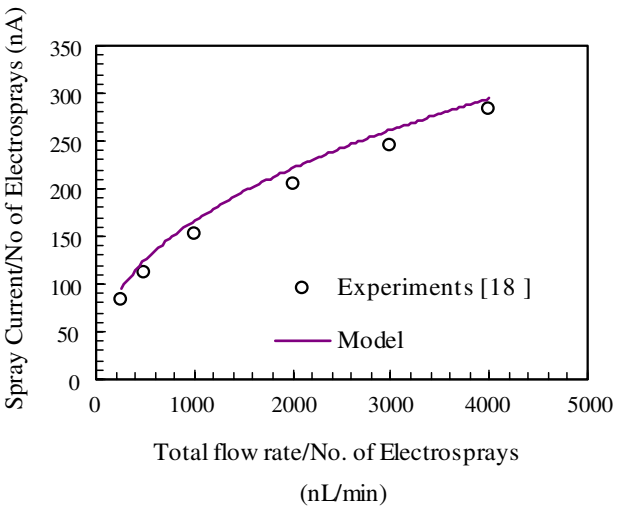

Fig. 8 Electrospray current as a function of flow rate

$$(I/n) = m_{IQ}(Q/n)^{n_{IQ}} \tag{14}$$

where n is the number of emitters in the array, m_{IQ} and n_{IQ} are constants. The value of n_{IQ} predicted by the model is 0.42 which matches well with 0.44 as measured from experiments. Both of the values are close to the theoretical value of 0.5, reported in the literature (Higuera 2004; De la Mora and Loscertales 1994; Ganan-Calvo 1997).

4 Carbon nanofiber (CNF) electrospray emitter

4.1 Description of computational model

The carbon nanofiber based computational model is shown in Fig. 9a. The model comprises an array of CNFs grown around the orifice of a thermoplastic capillary of internal diameter D. The CNFs are conical in shape with a base radius r and length h as shown in Fig. 9c. The radial pitch (Rp) and circumferential pitch (Cp) in the distribution of CNFs in the array is depicted in Fig. 9d. A thin conductive layer is used on the periphery to maintain electrical connection to the nanofiber array. A constant potential difference of V_o is maintained between the carbon fiber and the counter electrode, which is located at a distance L from the capillary tube terminus. The electrospray is produced by infusing a leaky-dielectric fluid of density ρ, viscosity μ, electrical conductivity σ dielectric constant k, and surface tension coefficient γ at a constant volumetric flow rate Q.

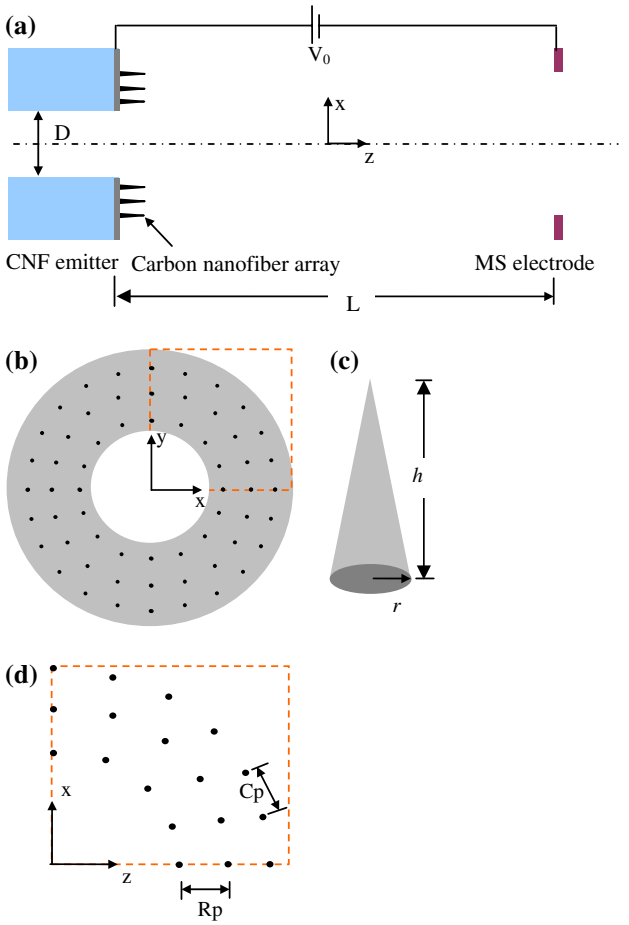

Fig. 9 **a** CNF emitter based model. **b** Array of CNFs on around the orifice, **c** geometry of an individual CNF, **d** Radial and circumferential pitch in the CNF array

4.2 Boundary condition

The boundary conditions for the CNF based model are similar to that described in section 3.1. However, in this case the high potential is applied to the carbon nanofiber array. The thermoplastic capillary tube is modeled as an insulator with a dielectric constant of 3.2.

4.3 Results and discussion

The configuration of the base model considered in the present simulation is as follows: D = 55 μm, d = 1,000 nm, l = 15 μm. The counter electrode is located at a distance of 0.4 mm from the nozzle (L = 0.4 mm). A potential difference of 1,200V was maintained between the carbon nanofiber array and the counter electrode for electrospraying a mixture of MeOH/H_2O/HOAc. Taking advantage of the symmetry of the emitter about x and y axis one-quarter of the emitter is considered for simulation as shown by the dotted lines in Fig. 9 (b).

Figure 10 shows a section (in x–y plane) of a 3-D mesh built around the model with (100, 100, 120) cells in (x, y, z) directions. In order to ensure that the results

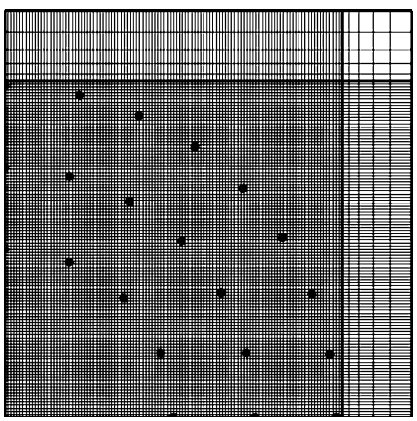

Fig. 10 Section (x–y) of a non-uniform 3-D mesh with (100, 100, 120) cells in (x, y, z) directions

are mesh independent, mesh convergence study was performed. The maximum electric field intensity as a function of total number of cells in the computational domain is shown in Fig. 11. The results indicate that the mesh in the computational domain is refined enough to achieve a good resolution. Figure 12 shows that the cells in the region containing the CNFs were small enough and a good resolution was achieved with cell size less than 0.4 μm in x- and y-directions. The jet diameter is defined at a section of the jet where it does not vary along the z-direction which was approximately 40 μm away from the tube terminus.

Figure 13 shows time evolution of the free surface of the cone-jet along with the electric potential contours in the computational domain. Due to interaction between the electrohydrodynamic forces, the liquid exiting the nozzle flows laterally towards the carbon nanofibers in the array. Liquid cones are formed around each of the carbon nanofibers. When the apex

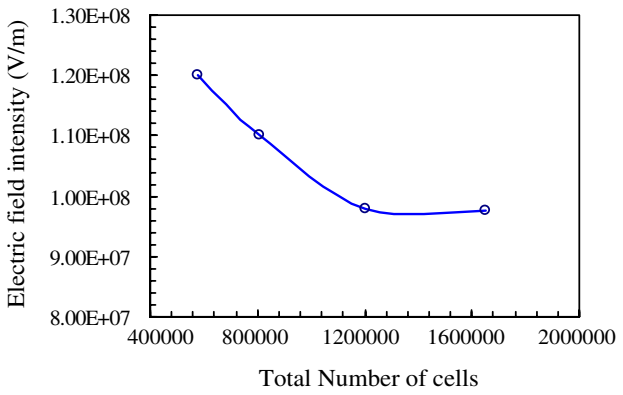

Fig. 11 Maximum electric field intensity versus total number of cells in the computational domain

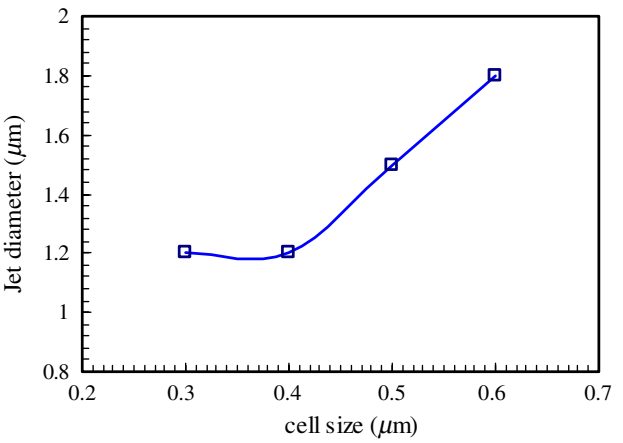

Fig. 12 Jet diameter versus minimum cell size in x and y directions near the jetting region

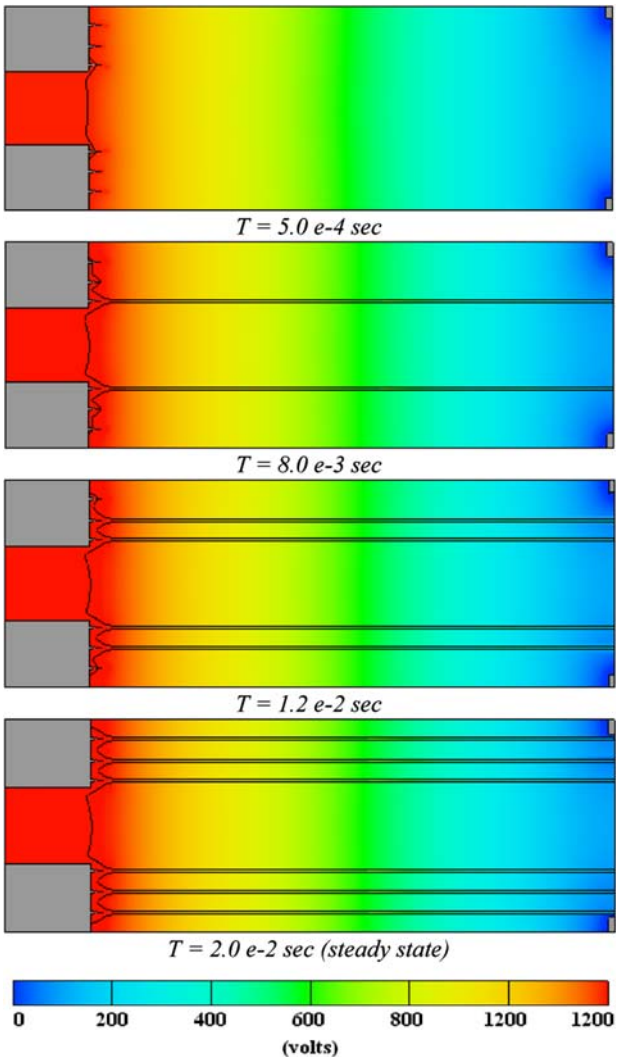

Fig. 13 Time evolution of cone-jet profiles and the electric potential contours in the computational domain

of Taylor cone profiles reach the sharp tips of the carbon nanofibers, liquid jets are evolved instantaneously and remain steady with time. The nanofiber located closer to the orifice delivers electrospray earlier than those located far form the orifice. Attainment of a steady state solution was ensured by observing no change in the potential distribution, electric field intensity, charge density, and velocity with time. A relative residue of 1.0×10^{-7} was specified in all simulations. In this particular case, the steady state was reached at time 2.0×10^{-2} s.

During the steady state the Taylor cones are confined to the sharp tip of the carbon nanofibers where the electric field is the highest. The electric field intensity contours presented in Fig. 14 show a large jump in the electric field across the free surface of the cone-jet profiles, which is responsible for the normal

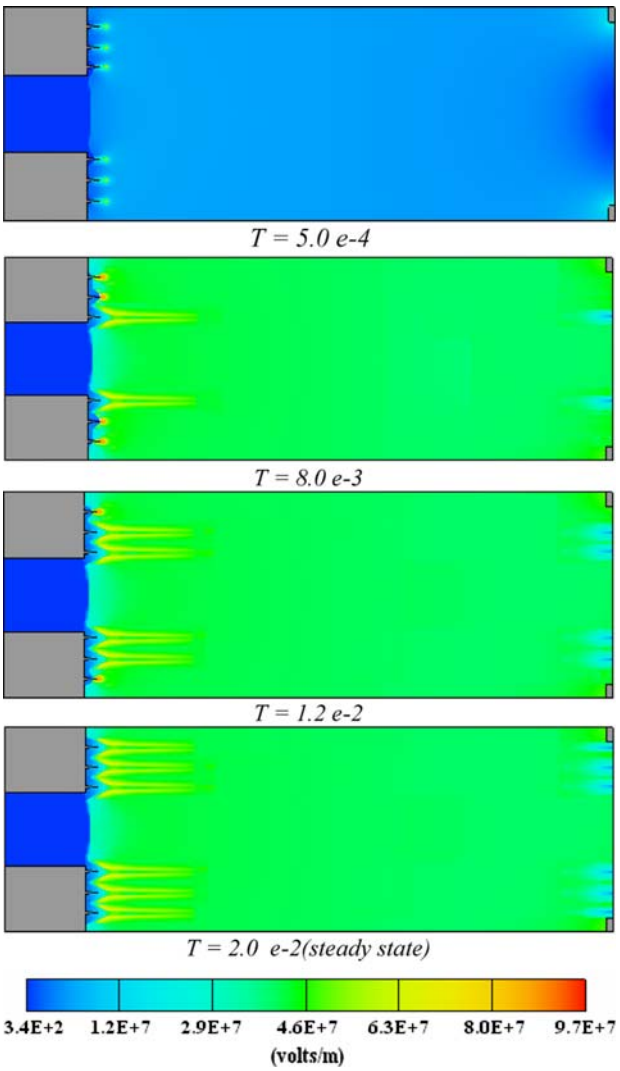

Fig. 14 Time evolution of electric field intensity contours in the computational domain

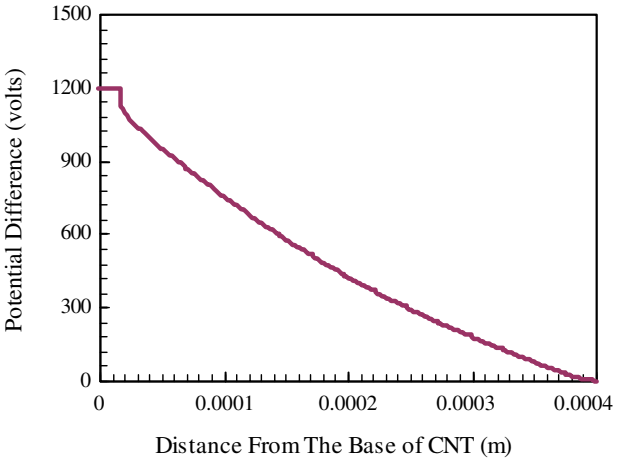

Fig. 15 Variation of electric potential along a cone-jet axis along z-direction

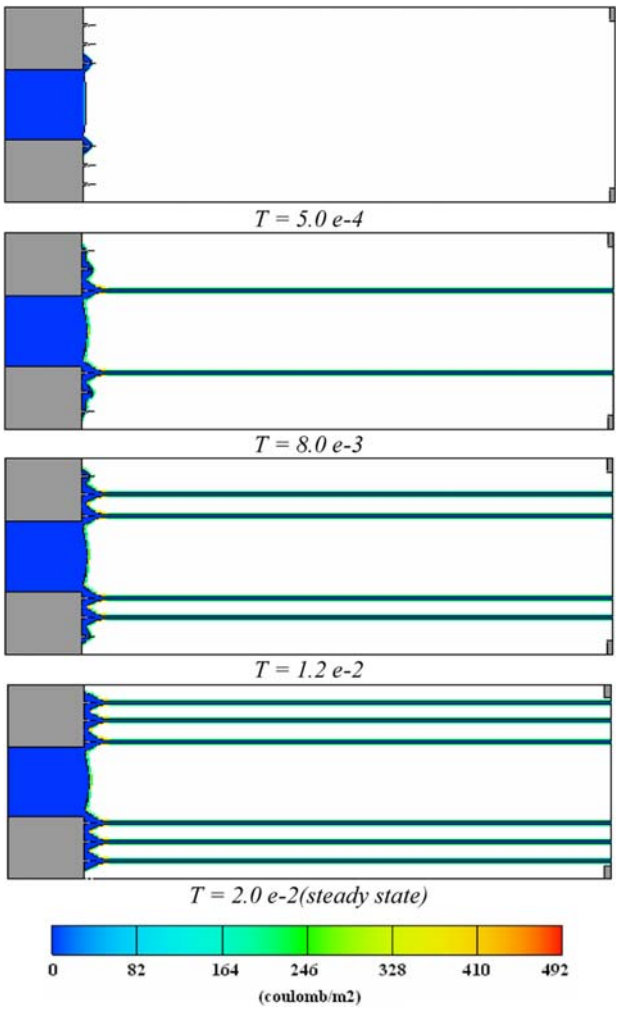

Fig. 16 Time evolution of charge density contours in the computational domain

and tangential electric stresses. The normal stress maintains the cone shape and the tangential stress accelerates the liquid towards the jet. The variation in the electric potential along a cone-jet axis is presented in Fig. 15. There is a large drop in the electric potential near the tip of the carbon fiber which results in a strong electric field at this region. The charge density contours on the cone-jet are shown in Fig. 16. As expected, the free charges are mainly accumulated near the interfacial region conforming to the leaky-dielectric model.

5 Parametric studies

In this section, influence of design and operational parameters on the electrospray performance of the CNF emitter is thoroughly investigated. The geometry

and distribution pattern of the carbon nanofibers in the array can affect the electrospray performance of the emitter and can be controlled during the micro-fabrication process. Electrospray performance of the emitter can be different for different solvents having different physical properties. From an electrospray performance perspective a higher spray current and lower jet diameter are desired. A higher spray current indicates ion abundance and therefore increases the chances of ion detection. A lower jet diameter results in a smaller primary droplet which can break easily into individual ions thus increasing the individual ion density. 'Onset' potential is the minimum potential required for generating steady electrosprays. A lower value of 'onset' potential is desired as it makes handling of the entire electrospray system easier. The volume of solvent present inside a Taylor cone is termed as dead volume as it never gets ionized. An electrospray with a smaller liquid cone is often stable and has less dead volume.

The aspect ratio (h/r ratio) of the individual CNFs is the most important design parameters that can influence the electrospray performance of the emitter. Based on the design, three types of variations in the geometry of CNFs is possible as shown in Fig. 17. Effects of these variations can be evaluated by studying the influence of aspect ratio for different values of radius.

Effects of aspect ratio on the maximum electric field strength are depicted in Fig. 18. As observed, for a fixed base radius, a higher aspect ratio gives rise to increased electric field strength and at a fixed aspect ratio, CNFs having smaller base radius generate higher electric field strength. Variation in 'onset' potential with aspect ratio is presented in Fig. 19. As expected, due to a higher electric field, a higher aspect ratio results in a lower 'onset' potential. For a fixed aspect ratio, the 'onset' potential is less for CNFs having smaller radius.

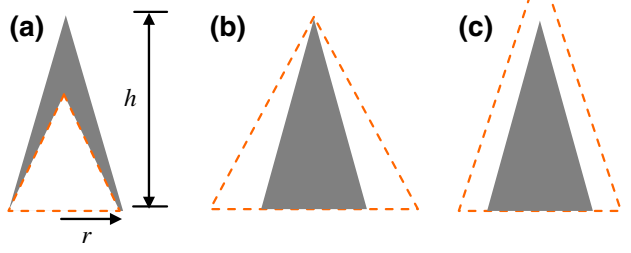

Fig. 17 **a** h varies with r remaining constant, **b** r varies with h remaining constant, **c** both h and r vary

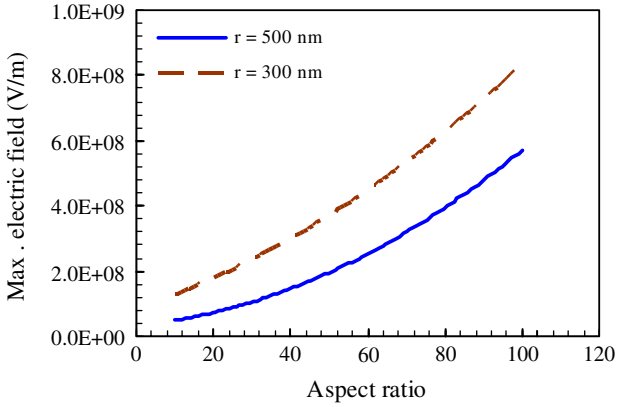

Fig. 18 Effects of aspect ratio (h/r) on electric field strength

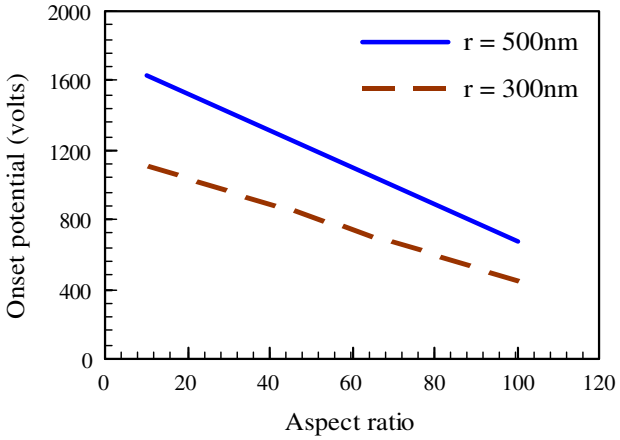

Fig. 19 Effects of aspect ratio (h/r) on 'onset' potential

Length of individual CNFs on the cone-length is studied and the results are shown in Fig. 20. Since the jet emanates near the tip of the carbon fiber where the electric field strength is the highest, the length of

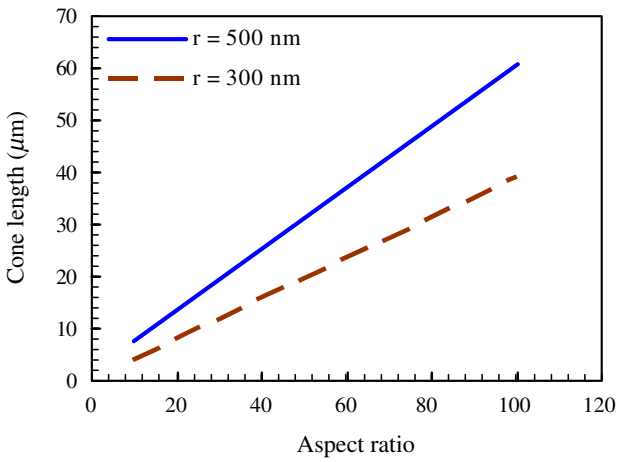

Fig. 20 Effects of aspect ratio (h/r) on cone-length

the cone increases linearly as the length of the CNFs. Therefore, for a fixed base radius, CNFs having higher length result in higher electric field and lower 'onset' potential but simultaneously CNFs of higher length also generate higher cone length and hence higher dead volume. Effects of surface tension of fluid on the 'onset' potential are studied in Fig. 21. A solvent of higher surface tension requires a higher onset potential. But higher aspect ratio of CNFs can electrospray solvents of higher surface tension at the same applied voltage. This is due to the fact that higher electric field obtained with high aspect ratio CNFs. Effects of aspect ratio on electrospray current and jet diameter are depicted in Fig. 22. As observed, electrospray current increases with increased aspect ratio which may be due to a high electric field achieved at a higher aspect ratio. Also, the jet diameter decreases with increase in aspect ratio, for a fixed based radius of CNFs. Effects of aspect ratio of CNFs on the possible range of operating flow rate for which a stable electrospray is possible is studied which is depicted in Fig. 23. As observed, the range of flow rate for which a stable electrospray is possible is higher for CNFs of higher aspect ratio.

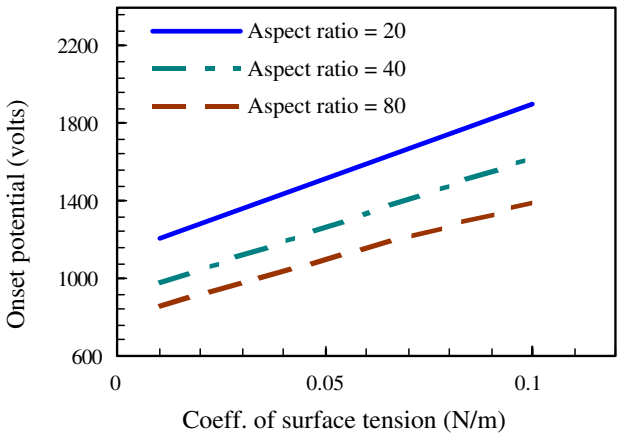

Fig. 21 Effects of aspect ratio (h/r) on 'onset' potential at different values of surface tension

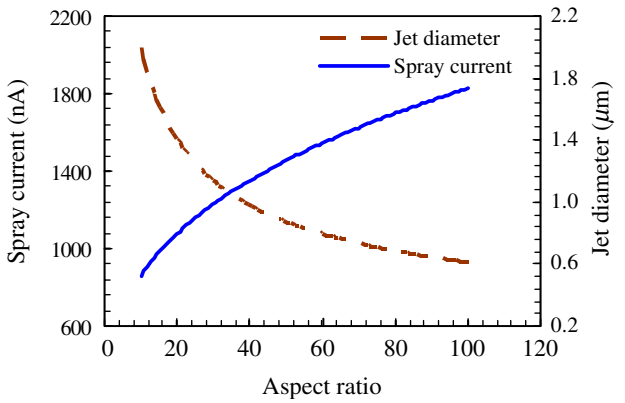

Fig. 22 Effects of aspect ratio (h/r) on electrospray current and jet diameter

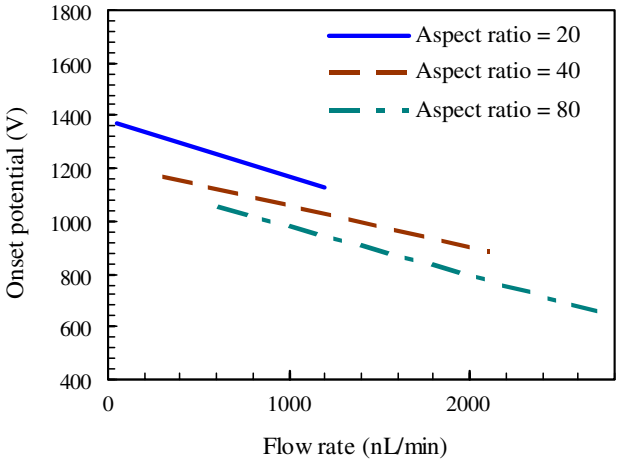

Fig. 23 Effects of aspect ratio (h/r) on the possible range of flow rate for a stable electrospray

The effects of the diameter of the capillary and the distance between the counter electrode and the tip of the CNF on the performance of the emitter are also investigated. Electrospray current and jet diameters were not affected but the 'onset' potential was reduced linearly with decrease in the gap between the emitter and the counter electrode which is expected theoretically.

The distribution of the CNFs around the orifice is another design parameter that can influence the electrospray performance of the emitter and can be controlled by varying the radial and circumferential pitch between the CNFs in the array. Effects of radial and

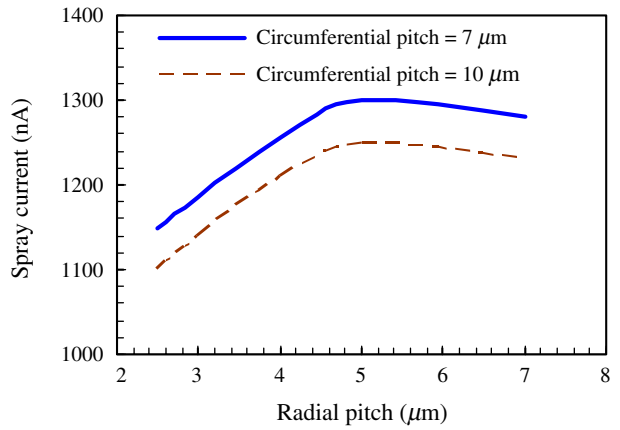

Fig. 24 Effects of radial pitch on electrospray current at different values of circumferential pitch

circumferential pitch of the distribution of CNF on the electrospray current are depicted in Fig. 24. With increase in the pitch, the electric field increases but the jet velocity and diameter are reduced. The electrospray current initially increases and then reaches the maxima after which it again decreases. Effects of the radial pitch of the distribution of nanofibers in the array on the 'onset' potential are presented in Fig. 25. Due to interaction between the cone-jets, the 'onset' potential increases as the radial gap between the nanofibers decreases. For a fixed radial gap, a lower circumferential gap results in a higher 'onset' potential. Increase in 'onset' potential with reduction in the gap between multiple electrospray emitters have been reported previously (Regele et al. 2002).

Another design parameter that can influence the electrospray performance is the total number of CNFs present in the array. Increase in total spray current with increase in total number of CNFs in the array is depicted in Fig. 26. Theoretical predictions of De la Mora and Loscertales (1994) and Ganan-Calvo et al. (1997) indicate that electrospray current from a single emitter is related to flow rate as follows,

$$I_n = f(\varepsilon)(Q_n \sigma\gamma/\varepsilon)^{1/2} \tag{15}$$

where,I_n and Q_n spray current from each electrospray and flow rate though each of the cone-jets, respectively. If there are N numbers of CNFs in the array, the total spray current becomes

$$I_{\text{total}} = \sum_{n=1}^{N} I_n \tag{16}$$

Assuming that liquid is uniformly distributed to each of the emitter (i.e. $Q_n = Q/N$), each electrosprays in the array will carry the same ion current. Therefore,

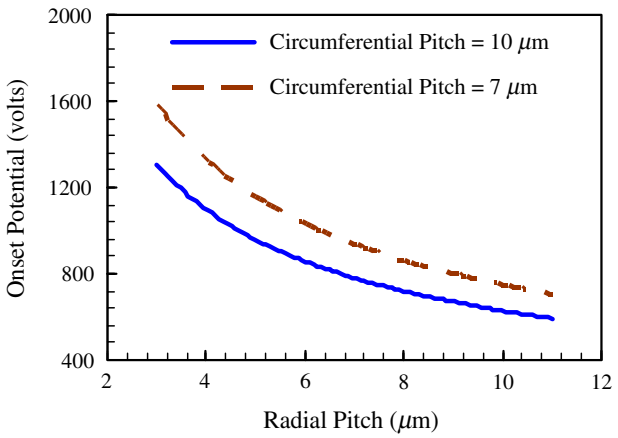

Fig. 25 Effects of radial pitch on the 'onset' potential

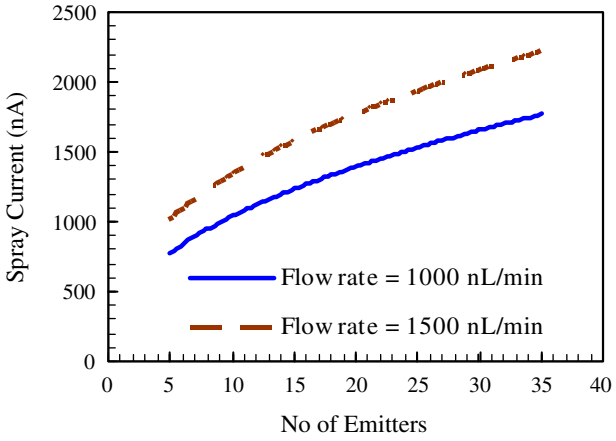

Fig. 26 Effects of no of emitters on the total electrospray current at different values of flow rate

$$I_{\text{total}} = N I_n \tag{17}$$

By substituting Eq. 17 in Eq. 15, we have

$$I_{\text{total}} = N f(\varepsilon)[(Q/N)(\sigma\gamma/\varepsilon)]^{1/2} = N^{0.5} I_s \tag{18}$$

where I_s is the ion current due to a single electrospray for the same total flow rate Q. Therefore, for a given flow rate, the total ion current is proportional to square root of number of electrosprays in the array. By correlating I_{total} and N in Fig. 26, the exponent of N was calculated to be 0.43 which matches the theoretically predicted value of 0.5 within 14%.

Additionally, electrospray current and flow rate were normalized with respect to the number of emitters. All the curves matched well indicating the validity of the assumptions that each of the electrosprays in the array carries the same flow and spray current. Effects of total number of CNFs on the average jet diameter and jet velocity are presented in Fig. 27. Jet diameter is reduced quadratically and jet velocity is reduced linearly with increase in the number of CNFs in the array.

Influence of several operational parameters such as flow rate, potential difference and physical properties of the solvent on the electrospray performance of the CNF emitter is thoroughly examined. Figure 28 depicts variation in 'onset' potential with the solvent flow rate. As observed, the 'onset' potential decreases with increase in flow rate and at a fixed flow rate the 'onset' potential is lower for a more conductive solvent. This trend is consistent with previously reported experimental observation (Cloupeau and Prunet-Foch 1989) as well as previous modeling works (Sen et al. 2006). Variation in electrospray current with respect to potential difference is studied. Figure 29 shows that

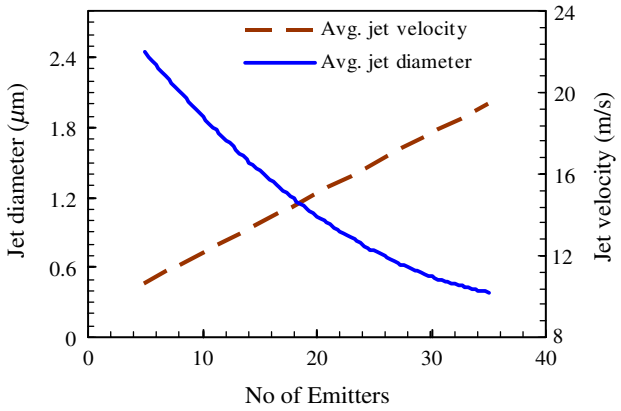

Fig. 27 Effects of no of emitters on the jet diameter and the jet velocity

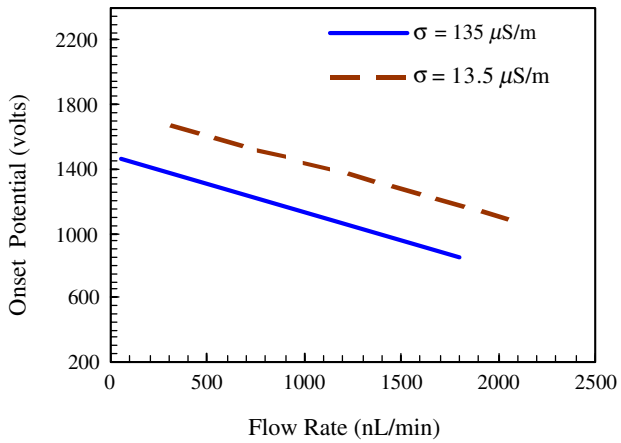

Fig. 28 Effects of flow rate on the 'onset' potential

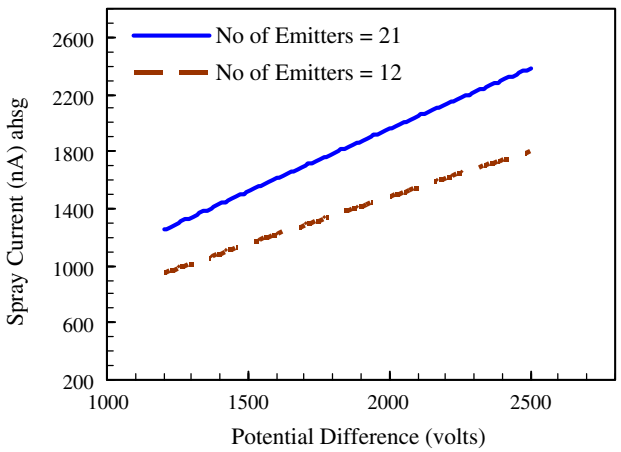

Fig. 29 Effects of potential difference on electrospray current at different no of emitters in the array

electrospray current increases approximately linearly with increase in potential difference. Electrospray current can be correlated with the potential difference as follows,

$$I = m_{\mathrm{IV}} V^{n_{\mathrm{IV}}} \tag{19}$$

The value of n_{IV} is calculated to be 0.88. Increase in the electrospray current with increase in the applied potential difference has been previously reported by Ganan-Calvo (1997). The value of n_{IV} was calculated to be 0.86 by Sen et al. (2006) both from the model and experiments.

Influence of solvent flow rate on the electrospray current and jet diameter is investigated. Figure 30 depicts that both electrospray current and jet diameter increase with increase in solvent flow rate. Spray current and jet diameter are correlated with flow rate and correlation results are presented in Table 1. A higher flow rate leads to lower onset potential and higher spray current. But simultaneously it gives rise to a higher jet diameter. An appropriate flow rate selection should be based on the sample availability and operating conditions. Effects of electrical conductivity, surface tension and viscosity of the solvent on electrospray current and jet diameter are investigated. As observed in Fig. 31, the spray current is higher and jet diameter is lower for a more conductive solvent. As shown in Fig. 32, the spray current increases and jet diameter decreases with increase in the surface tension of the solvent. Figure 33 presents decrease in spray current and increase in jet diameter with increase in the viscosity of the fluid. Similar trends have been reported previously (Hartman et al. 1999). Spray current and jet diameters are correlated with conductivity, surface tension and viscosity and the correlation results are presented in Table 1. As observed, the correlation

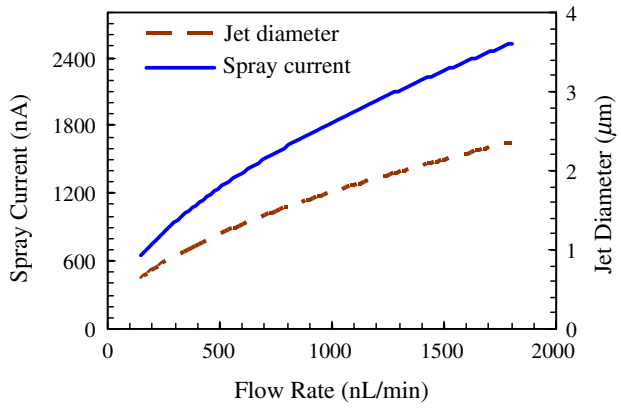

Fig. 30 Variation of electrospray current and jet diameter with flow rate

Table 1 Results of correlation between spray current and jet diameter with conductivity, surface tension and viscosity

Correlations	Correlation value	Model	Analytical (De la Mora and Loscertales 1994)	Analytical (Ganan-Calvo 1997)
Current (I)–flow rate(Q) $I = m_{IQ}\sigma^{n_{IQ}}$	n_{IQ}	0.564	0.5	0.5
Jet diameter (d)–flow rate(Q) $d = m_{dQ}d^{n_{dQ}}$	n_{dQ}	0.552	1/3	0.5
Current (I)–conductivity(σ) $I = m_{I\sigma}\sigma^{n_{I\sigma}}$	$n_{I\sigma}$	0.553	0.5	0.5
Jet diameter (d)–conductivity(σ) $d = m_{d\sigma}d^{n_{d\sigma}}$	$n_{d\sigma}$	– 0.185	– 1/3	– 1/6
Current (I)–surface tension(γ) $I = m_{I\gamma}\sigma^{n_{I\gamma}}$	$n_{I\gamma}$	0.582	0.5	0.5
Jet diameter (d)–surface tension(γ) $d = m_{d\gamma}\sigma^{n_{d\gamma}}$	$n_{d\gamma}$	– 0.181	–	– 1/6
Current (I)–viscosity(μ) $I = m_{I\mu}\sigma^{n_{I\mu}}$	$n_{I\mu}$	– 0.376	–	–
Jet diameter (I)–viscosity(μ) $d = a_{d\mu}\ln(\mu) + b_{d\mu}$	$a_{d\mu}, b_{d\mu}$	0.682, 2.42	–	–

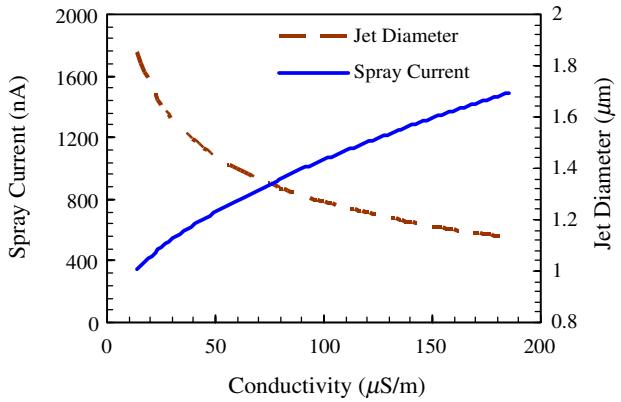

Fig. 31 Effects of solvent electrical conductivity on electrospray current and jet diameter

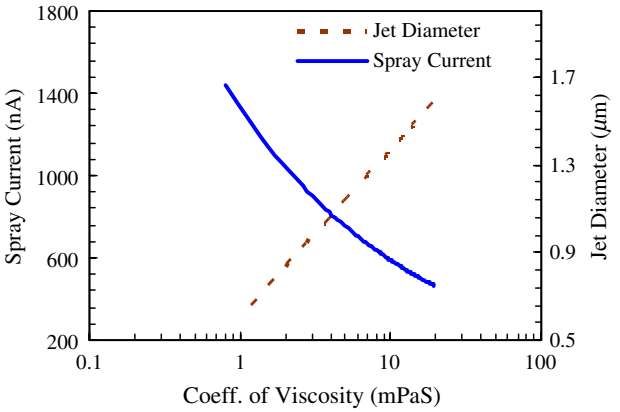

Fig. 33 Effects of viscosity of the solvent on the electrospray current and the jet diameter

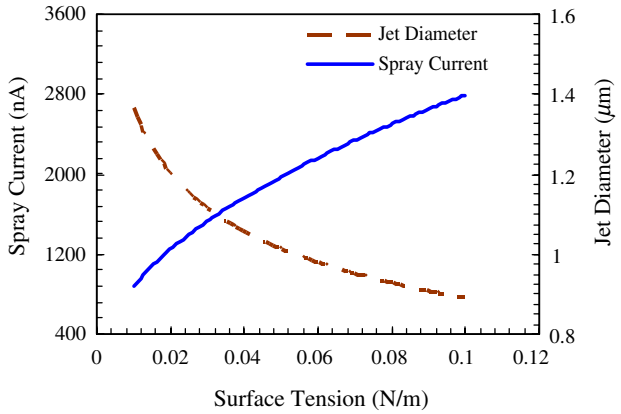

Fig. 32 Effects of surface tension of the solvent on electrospray current and jet diameter

results compare well with the available results in the literature.

6 Fabrication strategy

The proposed novel CNF emitter will be fabricated as part of a microfluidic device on a thermoplastic substrate. An open microchannel formed on a substrate by hot embossing will be bonded with a planar substrate to form a closed micro-channel that serves as the solvent capillary (Liu et al. 2006). This process produces rectangular channels. These channels will be made circular near the exit region (up to ~ 100 μm) using laser micromachining. This is to eliminate significant deviation in the Taylor cone shapes between a circular and rectangular orifice (Wang et al. 1999) and ensure a stable Taylor cone formation. The dimensions and the structure of the capillary will be analyzed using a scanning electron microscope (Fig. 35).

Arrays of circular dots (can be 100–1,000 nm diameter) will be defined in a circular grid pattern at 3–5 μm intervals around the capillary orifice. Nickel will be deposited as a growth catalyst layer on these spots using magnetron sputtering with an overlaid shadow mask produced by chemically etching a microlithographically pattered silicon wafer. This is pictorially shown in Fig. 35a. Vertically aligned carbon nanofibers will be grown out of the catalyst dots in a DC glow discharge chemical vapor deposition system using acetylene as the carbon source. Growth of carbon nanotubes on polymers substrates using PECVD has

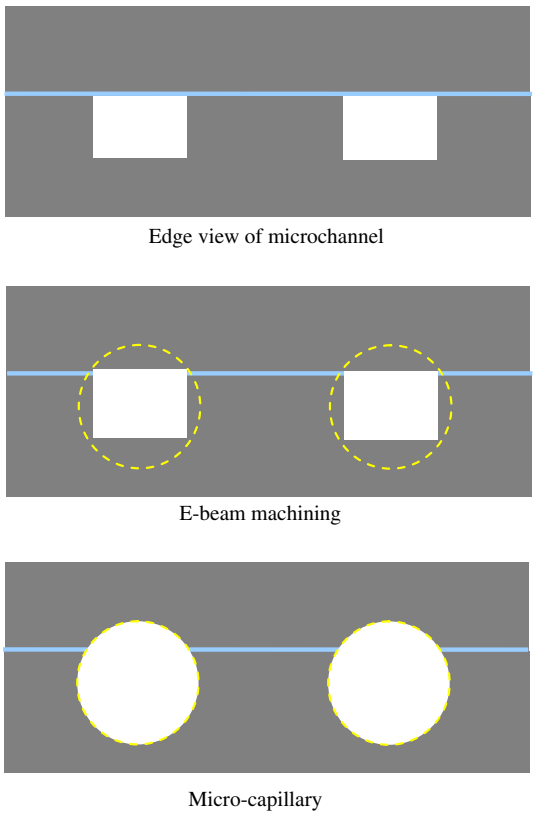

Fig. 34 Major process steps involved in the fabrication of the micro-capillary

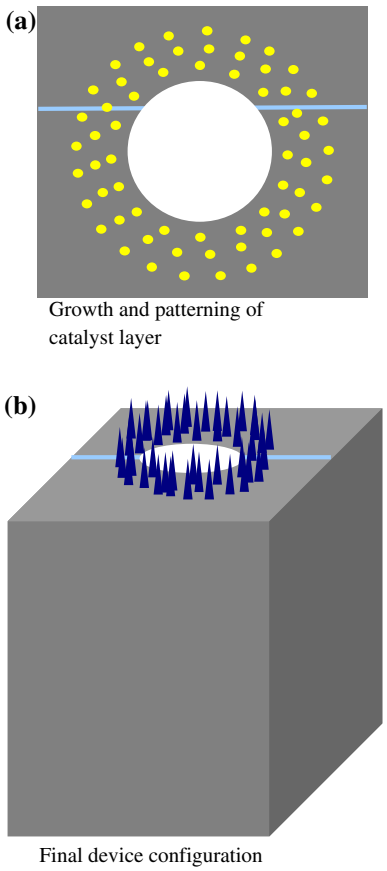

Fig. 35 **a** Nickel catalyst pattern on thermoplastic substrate. **b** Schematic of the CNF emitter

been demonstrated (Ryu et al. 2003). A schematic of the possible final configuration of the CNF emitter is shown pictorially in Fig. 35b.

7 Conclusions

A novel multiple electrospray emitter employing an array of carbon nanofibers around the orifice of a micro-scale thermoplastic capillary is proposed. The proposed emitter is simulated to evaluate its electrospray performance. The simulation results indicate that the emitter can generate steady state cone-jets from individual nanofibers forming an array of electrosprays. The emitter is observed to generate stable electrosprays for a wide range of flow rate, applied potential and liquid properties, thus making it suitable for electrospray–MS analysis. The electrospray performance of the novel emitter evaluated with respect to its geometry, operating conditions and physical properties of the liquid. The results indicate that aspect ratio of the CNFs is the most important design factor that affects the electrospray performance of the CNF emitter and an emitter with higher aspect ratio CNFs results in a higher electrospray current and requires lower 'onset' potential. The results also indicate that a smaller gap between the nanofibers requires a higher 'onset' potential. It was observed that the total spray current increases with increase in the total number of nanofibers. The spray current, 'onset' potential and jet diameter are correlated with number of CNFs and their distribution in the array, operational parameters and physical properties of the liquid. The correlation results are compared with the available results in literature. Higher spray current and lower jet diameter indicate that the device can perform equivalent to nanospray emitters while using a micro-scale orifice. This allows higher sample throughput and eliminates potential clogging problem inherent in nano-capillaries. The work is ongoing and efforts to fabricate the CNF emitter are underway. Once the device is fabricated, electrospray–MS experiments will be performed using the CNF emitter. Then the modeling and experimental results will be compared and the model can be improved, if required.

Acknowledgments Supported in part by a grant from the University of South Carolina Research and Productive Scholarship Fund, NIH grant CA86285 and the NHLBI proteomics Initiative via contract N01-HV-28181 (D.R.K.).

References

Amekinders JC, Jones C (1999) Multiple jet electrohydrodynamic spraying and applications. J Aerosol Sci 30:969–971

Amirkhani, A, Wetterhall M, Nilsson S, Danielsson R, Bergquist, J (2004) Comparison between different seathless electrospray emitter configurations regarding the performance of nanoscale liquid chromatography-time-of-flight mass spectrometric analysis. J Chromatogr A 1033:257–266

Arscott S, Le Gac S, Druon C, Tabourier P, Rolando C (2004)A planar micro-nib interface for nanoESI-MS microfluidic applications. J Micromech Microeng 14:310–316

Bocanegra R, Barrero A, Loscertales IG, Marquez M (2003) Multiplexing electrosprays emitted from an array of holes. In: 56th annual meeting of the division of fluid dynamics, Bull Am Phys Soc 48

Castellanos A (1998) Basic concepts and equations in electrohydrodynamics. In: Electrohydrodynamics, Springer, Berlin Heidelberg New York

Chhowalla M, Teo KBK, Ducati C, Rupesinghe NL, Amaratunga GAJ, Ferrari AC, Roy D, Robertson, J, and Milne WIJ (2001) Growth process conditions of vertically aligned carbon nanofibers using plasma enhanced chemical vapor deposition. Appl Phys Lett 90:5308

Clegg GA, Dole M (1971) Molecular beams of macroions. 3. Zein and polyvinylpyrrolidone. Biopolymers 10(5):821–826

Cloupeau M, Prunet-Foch B (1989) Electrostatic spraying of liquids in cone-jet mode. J Electrostat 22:135–59

De la Mora FJ, Loscertales IG (1994) The current emitted by highly conducting Taylor cones. J Fluid Mech 260: 155–184

Deng W, Li X, Klemic J, Reed M, Gomez A (2006) Increase of electrospray throughput using multiplexed microfabricated sources for the generation of monodisperse droplets. J Aerosol Sci 37:696–714

Dole M, Mack LL, Hines RL, Mobley RC, Ferguson LD, Alice MB (1968) Molecular beams of macroions. J Chem Phys 49:2240–2249

Duby MH, Deng W, Kim K, Gomez T, Gomez A (2006) Stabilization of monodisperse electrosprays in the multi-jet mode via electric field enhancement. J Aerosol Sci 37(3):306–322

Ebbesen TW, Ajayan PM (1992) Large-scale synthesis of carbon nanofibers. Nature (London) 358:220

Fenn, JB, Mann M, Meng CK, Wong SF, Whitehouse CM(1989) Electrospray ionization for mass spectrometry of large biomolecules. Science 246:64–71

Ganan-Calvo AM (1997) Cone–jet analytical extension of Taylor's electrostatic solution and the asymptotic universal scaling laws in electrospraying. Phys Rev Lett 79:217–220

Ganan–Calvo AM, Davila J, Barrero A (1997) Current and droplet size in the electrospraying of liquids. Scaling laws. J Aerosol Sci 28:249–275

Griss P, Melin J, Sjodahl J, Rocraade J, Stemme G (2002) Development of micromachined hollow tips for protein analysis based on nanoelectrospray ionization mass spectrometry. J Micromech Microeng 12:682–687

Hartman RPA, Brunner DJ, Camelot DMA, Marijnissen JCM and Scarlett B (1999) Electrohydrodynamic atomization in the cone-jet mode physical modeling of the liquid cone and jet. J Aerosol Sci 30:823–49

Higuera FJ (2004) Current/flow–rate characteristic of an electrospray with a small meniscus. J Fluid Mech 513:239–46

Hirt CW, Nichols BD (1981) Volume of fluid (VOF) method for the dynamics of free boundaries. J Comput Phys 39:201–225

Hofmann S, Ducati C, Kleinsorge B, and Robertson J (2003) Low-temperature growth of carbon nanofibers by plasma-enhanced chemical vapor deposition. Appl Phys Lett 83:135–137

Hofmann S, Ducati C, Kleinsorge B, Robertson J (2003) Direct growth of aligned carbon nanofiber field emitter arrays onto plastic substrates. Appl Phys Lett 83(22):4661–4663

Huberman MN, Beynon JC, Cohen E, Goldin DS, Kidd PW, Zafran S (1968) Present status of colloid microthruster technology. J Spacecr Rockets 5:1319–1324

J Liu, KW Ro, R Nayak, DR Knapp (2006) Monolithic column plastic microfluidic device for peptide analysis using electrospray from a channel opening on the edge of the device. Int J Mass Spectrom (in press)

Jian L, Kyung WR, Mark B, and Knapp DR (2004) Electrospray Ionization with a pointed carbon fiber emitter. Anal Chem 76:3599–3606

Kaiser S, Kyritsis DC, Dobrowolski P, Long MB, Gomez A (2003) The electrospray and combustion at the mesoscale. J Mass Spectrom 51(1):42–49

Kim JS, Knapp DR (2001) Microfabrication of polydimethylsiloxane electrospray ionization emitters. J Chromatogr A 924:137–145

Melcher J R (1981) Continuum electromechanics. MIT Press, Cambridge

Melechko AV, McKnight TE, Hensley DK, Guillorn MA, Borisevich AY, Merkulov VI, Lowndes DH, Simpson ML (2003) Large scale synthesis of high-aspect-ratio rigid vertically aligned carbon nanofibers. Nanotechnology 14:1029–1035

Merkulov VI, Lowndes DH, Wei YY, Eres G, and Voelkl E (2000) Patterned growth of individual and multiple vertically aligned carbon nanofibers. Appl Phys Lett 76:3555

Regele JD, Papac MJ, Rickard MJA, Dunn-Rankin D (2002) Effects of capaillary spacing on EHD spraying from an array of cone jets. J Aerosol Sci 33:1471–1479

Ren ZF, Huang ZP, Xu JW, Wang JH, Bush P, Siegal MP, Provencio PN (1998) Synthesis of large arrays of well-aligned carbon nanofibers on thermoplastic. Science 282:1105–1107

Rulison AJ, Flagan R (1993) Scale-up of electrospray atomization using linear arrays of Taylor cones. Rev Sci Instrum 64:683–686

Ryu K, Kang M, Kim Y, Jeon H (2003) Low temperature growth of carbon nanotube by plasma-enhanced chemical vapor deposition using nickel catalyst. Jpn J Appl Phys 42:3578–3581

Saville DA (1997) Electrohydrodynamcis: the Taylor–Melcher leaky dielectric model. Annu Rev Fluid Mech 29:27–64

Schultz GA, Corso TN (2000) Proceedings of the 47th ASMS Conference on mass spectrometry and allied topics, Long Beach

Sen AK, Darabi J, Knapp DR, Liu J (2006) Modeling and characterization of a carbon fiber emitter for electrospray ionization. J Micromech Microeng 16:620–630

Tang K, Lin Y, Matson DW, Kim T, Smith RD (2001) Generation of multiple electrosprays using microfabricated emitter arrays for improved mass spectrometric sensitivity. Anal Chem 73:1658–1663

Thess A, Lee R, Nikolaev DH, Petit P, Robert J, Xu C, Lee YH, Kim SG, Rinzler AG, Colbert DT, Scuseria GE, Tomanek D, Fischer JE, Smalley RE (1996) Crystalline ropes of metallic carbon nanofibers. Science 273: 483

Trapp O, Pearce EW, Kimmel JR, Yoon OK, Zuleta IA, Zare RN (2005) A soft on-column metal coating procedure for robust seathless electrospray emitters used in capillary electrophoresis-mass spectrometry. Electrophoresis 26:1358–1365

Wang XQ, Desai A, Tai YC, Licklider L, Lee TD (1999) Polymer based electrospray chips for mass spectrometry. In: Proceedings of the IEEE micro electro mechanical systems (MEMS), Orlando, pp 523–528

Wang YX, Cooper JW, Lee CS, DeVoe DL (2004) Efficient electrospray ionization from polymer microchannels using integrated hydrophobic membranes. Lab Chip 4:363–367

Yoon SS, Heister SD, Epperson JT, Sojka PE (2001) Modeling multi-jet mode electrostatic atomization using boundary element methods. J Electrostatics 50(2):91–108

Zeleny J (1914) Phys Rev 3:69–91

Zeleny J (1917) Phys Rev 10:1–6